

Article

Effects of Magmatic-Hydrothermal Activities on Characteristic of Source Rocks from Beipiao Formation in the Jinyang Basin, NE China

Shuo Deng ^{1,2} , Sumei Li ^{1,2,*}, Shouliang Sun ^{3,*}, Ziyang Hao ⁴, Menghua Qin ⁴ and Yongfei Li ³

¹ State Key Laboratory of Petroleum Resources and Prospecting, China University of Petroleum, Beijing 102249, China; ds901007@163.com

² College of Geoscience, China University of Petroleum, Beijing 102249, China

³ Shenyang Center of China Geological Survey, Shenyang 110034, China; geology198086@163.com

⁴ Research Institute of Exploration and Development, Petrochina Huabei Oilfield, Renqiu 062550, China; yjy_hzy@petrochina.com.cn (Z.H.); yjy_qmh@petrochina.com.cn (M.Q.)

* Correspondence: smli@cup.edu.cn (S.L.); ssl_email@126.com (S.S.)

Abstract: The Jinyang Basin is a typical volcanic-sedimentary basin, located in the southern peripheral area of the Songliao Basin. Hydrothermal activity is often closely related to the intrusion or eruption of magma. It was recently suggested that dolomite in the Jurassic Beipiao Formation was formed under the influence of magmatic-hydrothermal activity and magmatic-hydrothermal activity might have impacts on the organic matter of the source rocks. No investigation has been aimed at the effect of magmatic-hydrothermal activities on the accumulation of organic matter in the Beipiao Formation source rocks and a comprehensive study is urgent, which would be indicative in unravelling the accumulation mechanism of organic matter and useful in further petroleum exploration. To provide important insights into these issues, we carried out a detailed investigation of geological and geochemical analysis for Wolong (WL) and Dongkuntouyingzi (DK) outcrop shales from the Lower Jurassic Beipiao Formation in the Jinyang Basin. The hydrothermal indicator discrimination diagram (Zn-Ni-Co triangular plot) and rare earth element anomalies (δEu and δCe) indicate that the formation of WL samples is associated with hydrothermal activity, but DK is not. The TOC values suggest that most of the WL and DK samples are good to very good and fair to good source rocks, respectively. The Ro values suggest that both WL ($R_o = 1.17\%$) and DK ($R_o = 1.01\%$) samples have entered the oil-generating stage, and WL samples were influenced by the magmatic activity with higher maturity. The biomarkers such as high steranes/hopanes, high 4-methyl steranes/ C_{29} steranes, low Pr/Ph values and high gammacerane index suggest that WL samples were deposited in an anoxic-prone saline environment with significant contributions of algal sources. Contrarily, the DK samples were deposited in oxic-prone and freshwater paleolake with significant contributions of terrigenous organic matter. The magmatic-hydrothermal activities in the Wolong area brought numerous nutrients to the lake basin, which may facilitated the reproduction of aquatic organisms. At the same time, the magmatic-hydrothermal activities increased the salinity of water and promoted the formation of a water reducing environment, which provided an excellent environment for the preservation and enrichment of organic matter. Therefore, the magmatic-hydrothermal activities in the Wolong area promoted the formation of organic-rich source rocks and the hydrocarbon generation process.

Keywords: magmatic-hydrothermal activity; organic matter enrichment; hydrocarbon generation; source rocks; Jinyang Basin



Citation: Deng, S.; Li, S.; Sun, S.; Hao, Z.; Qin, M.; Li, Y. Effects of Magmatic-Hydrothermal Activities on Characteristic of Source Rocks from Beipiao Formation in the Jinyang Basin, NE China. *Minerals* **2022**, *12*, 947. <https://doi.org/10.3390/min12080947>

Academic Editors: Gianreto Manatschal and Thomas Gentzis

Received: 27 April 2022

Accepted: 24 July 2022

Published: 27 July 2022

Publisher's Note: MDPI stays neutral with regard to jurisdictional claims in published maps and institutional affiliations.



Copyright: © 2022 by the authors. Licensee MDPI, Basel, Switzerland. This article is an open access article distributed under the terms and conditions of the Creative Commons Attribution (CC BY) license (<https://creativecommons.org/licenses/by/4.0/>).

1. Introduction

Massive magmatic-hydrothermal activities are widely distributed in numerous sedimentary basins worldwide [1,2]. Numerous basins with a large volume of magmatic-hydrothermal activities are petroliferous and targeted for hydrocarbon exploration, e.g.,

the Vøring Basin in the Norwegian margin [3,4] and the Tunguska Basin in Siberia [5]. The interactions of magmatic activities with their organic-rich host rocks have significant consequences for petroliferous systems [6]. The heating effect of organic-rich rocks by magmatic activities can result in maturation and even overmaturation [1,4,7–11]. Large quantities of hydrocarbons can be catastrophically released into the atmosphere, affecting the global climate [4,12]. In addition, structures induced by the emplacement of intrusions may generate fluid channels or fluid traps [13–16].

Thermal maturation effects of magmatic activities on source rocks have been well described and exhibit a range of maturity that varies with the number of intrusions, spacing, thickness, composition, length and distances between the intrusions and host rock [17,18]. The extent of the thermal aureole range mainly from 30% to 200% of the intrusion thickness [7,9,19–22]. The following observations have been reported that total organic carbon (TOC) and parameters derived from Rock-Eval pyrolysis (S_1 , S_2 and HI) have a gradual decrease, as the distance between the source rock and the intrusions decreases [9,22]. Recently, Sydnes [23] and Spacapan [18] demonstrated that the timing of magmatic activities emplacement is the controlling factor on host rock maturation.

Hydrothermal activity is often closely related to the intrusion or eruption of magma [24–26]. Magmatic hydrothermal plays an important role in the enrichment of organic matter, as well as the formation and evolution of source rocks in sedimentary basins [27–29]. Magma upwelling can release a large number of elements such as C, N, P, and Fe, which promotes the prosperity of biological water and increases primary productivity. It provides rich material basis for the formation of organic-rich source rocks [28–30]. The CO_2 in the magmatic hydrothermal reacted with the Ca^+ and Mg^{2+} plasma in the seawater to form carbonates, which increased water salinity and promoted the water stratification, creating favorable water dynamic conditions and redox state for the enrichment and preservation of organic matter [28,29]. Simultaneously, a large amount of CO_2 , CH_4 , SO_2 and other gases are released by magmatic hydrothermal activity form a reduced environment, which is favorable for the preservation of organic matter. Reducing gases such as H_2S and CO dissolved in water can also promote the formation of a reducing environment in the water [29,31].

Jurassic magmatic-hydrothermal activities were extensive and widespread in north-eastern China [32]. The Jinyang Basin is a typical volcanic-sedimentary basin, located in the southern peripheral area of the Songliao Basin. Preliminary studies indicated that Jinyang Basin is a petroliferous basin with huge potential and the Lower Jurassic Beipiao Formation shale has been proved to be the prime source rock [33–35]. There are many magmatic rock bodies developed in the source rock series of the study area. Some magmatic intrusions were emplaced in Beipiao Formation outcrops, especially in the Wolong and Dongkuntouyingzi areas [36]. Sun [37] proposed that the magmatic activity has a significant influence on the maturity of Beipiao Formation source rocks. Recently, Mou [38] suggested that dolomite in the Jurassic Beipiao Formation was formed under the influence of magmatic-hydrothermal activity, and the magmatic-hydrothermal activity might impact the organic matter of the source rocks. No investigation was aimed at the effect of magmatic-hydrothermal activities on the accumulation of organic matter in the Beipiao Formation source rocks and a comprehensive study is urgent, which would unravel the accumulation mechanism of organic matter and prove valuable in further petroleum exploration. Geological and geochemical analyses were conducted in the study for the purpose of discussing the above issues.

2. Geological Settings

The Jinyang Basin, tectonically bounded by the Nantianmen thrust fault to the west and the Songlingmen uplift to the east, is a recently discovered petroliferous basin located in the peripheral area of the well-known Songliao Basin, Northeast China (Figure 1). In the process of tectonic evolution, controlled by the tectonic sedimentary cycle of the second stage of the Yanshan Movement [39], the basin began to stretch after the volcanic

eruption of the Lower Jurassic Xinglonggou Formation, forming an early synsedimentary sag-controlling fault [36]. After the Beipiao-Haifanggou Formation was deposited, the Tijishan Formation erupted and the basin continued to stretch [36]. When the Yixian Formation volcanic erupted in the late Jurassic, the basin was strongly compressed and twisted, forming the Nantianmen fault zone. The fault zone divided the large basin into Beipiao and Jinyang Basins during the depositional period of the Upper Jurassic Beipiao Formation, forming the present tectonic pattern [40,41]. The basin, characterized by its northeastern elongated shape, is one of the Mesozoic volcano-sedimentary basins, which are widely distributed in the northern part of the north China craton [40,42,43]. However, according to studies in recent years, the shape of the basin during the Early Jurassic was an E–W trend [44,45]. The Yanshanian orogeny reshaped the basin during the middle-to-late Jurassic periods. The residual sedimentary strata in Jinyang Basin are mainly composed of Jurassic strata (Figure 1), with a thickness of up to 5000 m, including the Proterozoic, Carboniferous, Permian, Triassic, Jurassic and Cretaceous from the bottom to top.

Four geological survey wells (SZK01-04) were drilled on the western margin of the Jinyang basin, where oil and gas were encountered [46]. The YD-1 well drilled in the Zhangjiyingzi depression of the basin encountered oil spots in the fractures of volcanic rocks. Based on biomarker and source rock correlation studies, crude oil was derived from the Jurassic Beipiao Formation [47]. The total thickness of the Beipiao Formation in the core ZK01 reaches 280 m. The sedimentary paleoenvironment of the lower Beipiao Formation is composed of alluvial and lacustrine facies, which are characterized by coarse-grained, weakly cemented conglomerate, conglomeratic sandstone, siltstone and dark claystone interbedded with coal seams [33,48]. These sediments overlay directly on Lower Jurassic andesite or Precambrian carbonates. The upper part is by sandstone, siltstone and dark claystone interbedded with fine conglomerates [33,48]. However, only a few outcrops of the Beipiao Formation can be found in the Jinyang basin, with the majority of the outcrops occurring in the western area near the Nantianmen thrust fault, e.g., Wolong outcrop and Dongkuntouyingzi outcrops. The source rocks of the Beipiao Formation were influenced by magmatic-hydrothermal activities during the forming process [38]. A diorite porphyrite dike (U-Pb age: 173.4 ± 0.65 Ma, unpublished data), with a surface outcropping width of approximately 130 m, intruded into the bottom of the Wolong outcrop. A granite porphyry dike (U-Pb age: 172.6 ± 1.3 Ma) [49] with a surface outcropping width of approximately 80 m intruded into the top of the Dongkuntouyingzi outcrop. The dike also intruded into the middle of the Wolong outcrop, with a surface outcropping width of approximately 200 m (Figure 2). The sedimentary age of the Beipiao Formation is from the late Early Jurassic to early Middle Jurassic [50,51]. The motley strata at the bottom of the Beipiao Formation belong to the late Early Jurassic, and the dark coal-bearing strata at the middle-upper part belong to the early Middle Jurassic [50]. Therefore, the diorite porphyrite dike might intrude during the deposition of the dark coal-bearing strata in the Beipiao Formation, affecting the primary productivity and the preservation conditions of organic matter. Both outcrops provide a natural laboratory to study the interactive mechanism between the magmatic-hydrothermal activities and the Beipiao source rocks.

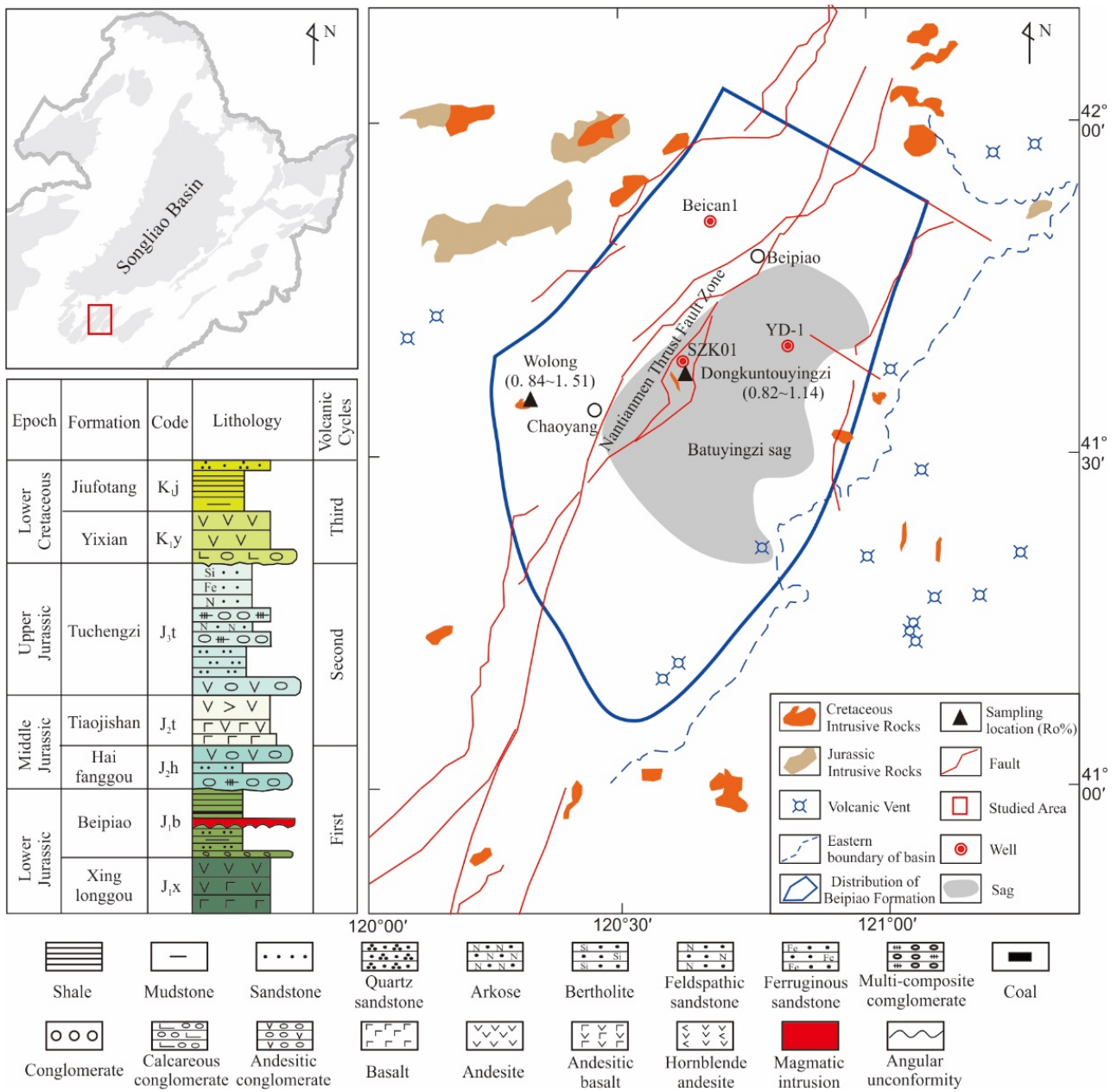


Figure 1. Location of the study area and the distribution of Jurassic and Cretaceous magmatic activities.

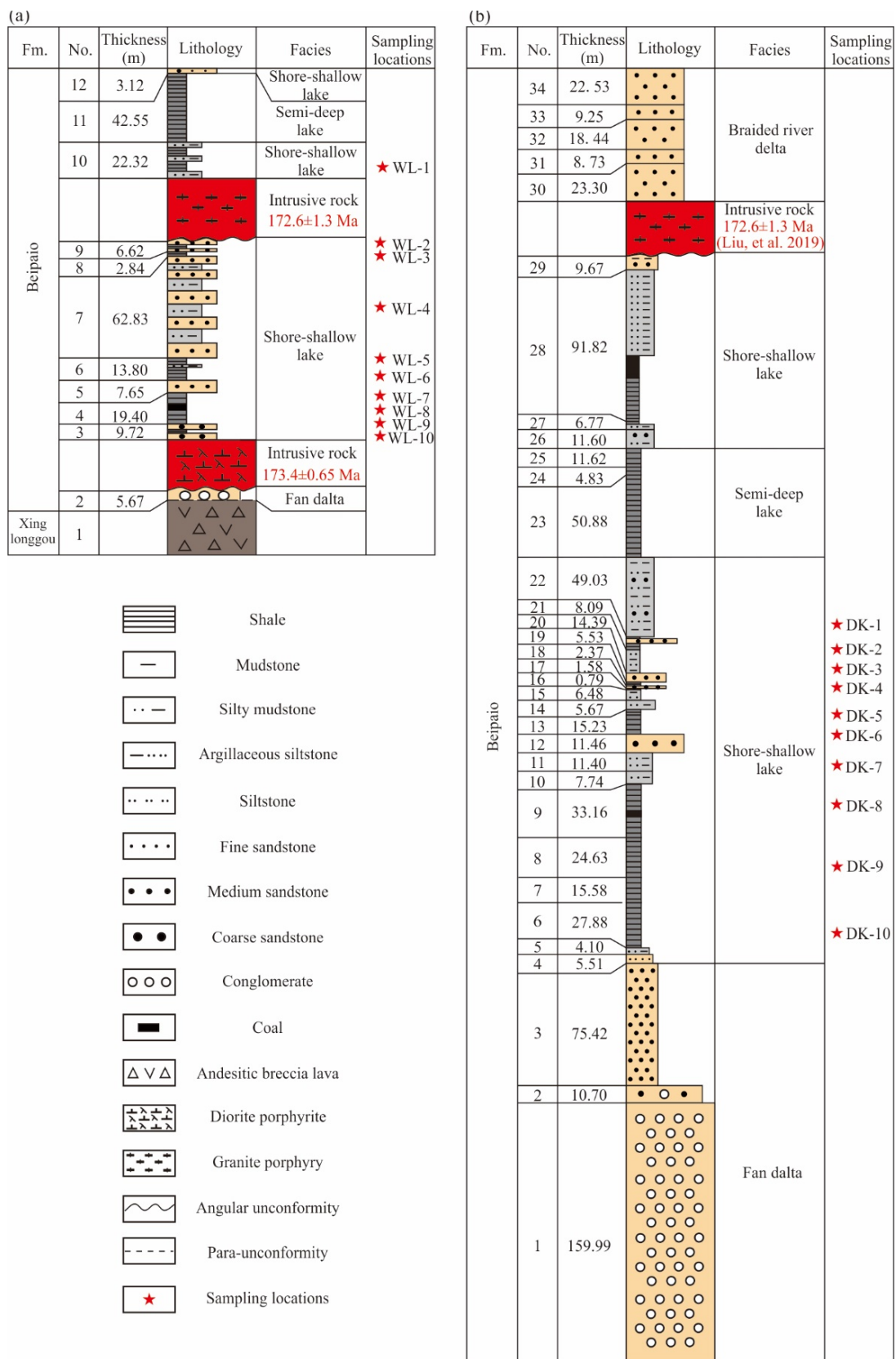


Figure 2. (a) Column of the Beipiao Formation in the Wolong outcrop, (b) Column of the Beipiao Formation in the Dongkuntouyingzi outcrop.

3. Samples and Methods

Twenty black shale samples in this study were collected from the Wolong (WL) outcrop in the west of Jinyang Basin (10 samples) and the Dongkuntouyingzi (DK) outcrop in the middle of Jinyang Basin (10 samples) (Figure 2). All samples are from the Beipiao Formation. The samples of the Wolong outcrop were collected from the vicinity of the granite porphyry dike, and gradually moved away from the dike at intervals of 20–50 m. All samples from both outcrops were collected from fresh surfaces to avoid the effects of biodegradation and weathering.

For total organic carbon (TOC) analysis, aliquots (~200 mg) of shale powders were first treated with 6 mol/L hydrochloric acid (HCl) at 60 °C for 12 h twice to remove carbonate minerals. Samples were then washed with distilled water to remove HCl, dried overnight (50 °C), and weighed. They were then measured using a LECO CS230 apparatus. Rock–Eval pyrolysis was performed with a Rock–Eval 6 instrument. The temperature program started with an isothermal phase for 3 min at 300 °C, followed by a heating step up to 650 °C at a rate of 25 °C.

The GC/MS analyses were carried out with an Agilent Technologies 7890A gas chromatograph coupled with an Agilent Technologies 5975C mass spectrometer. For the biomarker analysis, selected ions were chosen to analyze samples in single ion monitoring (SIM) or multiple ion detection (MID) mode. The ion source operated in the electron impact mode with energy of 70 eV. The GC was equipped with a 30 m × 0.32 mm (i.d.) J&W Scientific DB-5MS fused silica capillary column coated with a 0.25 µm liquid film. For the saturate and aromatic compounds analysis, the ion source temperature was 200 °C, injector temperature was at 300 °C, and transfer line temperature was 310 °C. The GC temperature program started at 40 °C and was held for 1.5 min, before being increased to 300 °C at a rate of 4 °C per minute and then held at 300 °C for 34 min (total run time of 100.5 min).

The trace elements and rare earth elements were analyzed and tested in the Yangtze University, China, with a Thermo Scientific Element XR inductively coupled plasma mass spectrometer. During the experiment, 10 ng Rh was used as the online internal standard, and the repeated measurement of the laboratory rock standard sample was used to control the analysis accuracy. The analysis error of trace elements is less than 5%, and the analysis error of rare earth elements is less than 10%. To eliminate the odd-even effect of REE, we adopted the Post-Archean Australian Shale (PAAS) for REE normalization.

Available data of vitrinite reflectance (%Ro) for some samples from this well were available and provided by the Key Laboratory of Exploration Technologies for Oil and Gas Resources at Yangtze University.

4. Results

4.1. Total Organic Carbon and Rock-Eval Pyrolysis

The WL samples have TOC values ranging from 0.61% to 3.20% (averaging 2.01%). A total of 88% of samples have moderate-to-good TOC content (TOC > 1.0%) [52]. The free hydrocarbon contents (S_1) and pyrolysis hydrocarbon (S_2) are generally low (averaging 0.05 mg/g and 0.11 mg/g, respectively). The Tmax values vary in a range of 427–573 °C (averaging 589 °C). The Ro values are in the range of 0.84–1.51% (averaging 1.17%) (Table 1).

The DK samples have TOC values between 0.65% and 3.27% (averaging 1.63%). A total of 70% of samples have moderate-to-good TOC content (TOC > 1.0%) [52]. The free hydrocarbon contents (S_1) and pyrolysis hydrocarbon (S_2) are generally low (averaging 0.15 mg/g and 0.98 mg/g, respectively). The Tmax values are in the range of 444–470 °C (averaging 449 °C). The Ro values range from 0.82 to 1.14% (averaging 1.01%) (Table 1).

4.2. Rare Earth Elements

In the WL samples, there is a positive correlation between the total rare earth element content (Σ REE) and TOC (Tables 1 and 2). The Σ REE decreased from 319.79 µg/g to 226.83 µg/g as the TOC content decreased. Chondrite normalized REE distribution patterns are uniformly light-REE (La–Nd) enriched, show a large positive Eu anomaly

($\delta\text{Eu} > 1$) and negative Ce anomaly ($\delta\text{Ce} < 1$) (Table 2). The data are consistent with REE compositions previously reported for Vienna Woods hydrothermal fluids [53,54] and Tarim Basin hydrothermal fluids [55]. In the DK samples, most of them exhibit a negative Eu anomaly ($\delta\text{Eu} < 1$) and positive Ce anomaly ($\delta\text{Ce} > 1$) (Table 2).

Table 1. Experimental results of Rock-Eval analysis and TOC measurement for source rocks.

Sample No.	Fm.	Lithology	Distance (m)	TOC (%)	S ₁ (mg/g)	S ₂ (mg/g)	Tmax (°C)	HI (mg/g)	OI (mg/g)	Ro (%)
WL-1	J ₁ b	Shale	29.00	2.18	0.09	0.19	573.00	8.72	216.06	1.45
WL-2	J ₁ b	Shale	46.00	3.20	0.05	0.12	558.00	3.75	184.38	1.51
WL-3	J ₁ b	Shale	94.00	2.90	0.03	0.08	531.00	2.76	160.34	1.43
WL-4	J ₁ b	Shale	114.00	2.57	0.06	0.15	447.00	5.84	163.04	0.97
WL-5	J ₁ b	Shale	150.00	1.29	0.11	0.19	471.00	14.73	430.23	1.13
WL-6	J ₁ b	Shale	250.00	1.63	0.03	0.04	427.00	2.45	142.94	0.84
WL-7	J ₁ b	Shale	300.00	1.68	0.04	0.10	430.00	5.95	110.71	0.86
WL-8	J ₁ b	Shale	335.00	0.61	0.02	0.03	472.00	4.96	345.45	1.14
WL-9	J ₁ b	Shale	380.00	-	-	-	-	-	-	-
WL-10	J ₁ b	Shale	396.00	-	-	-	-	-	-	-
DK-1	J ₁ b	Shale	280.00	0.87	0.13	0.61	444.00	70.36	144.18	1.11
DK-2	J ₁ b	Shale	310.00	0.65	0.06	0.28	444.00	43.28	194.74	1.14
DK-3	J ₁ b	Shale	340.00	0.95	0.25	1.08	447.00	114.04	180.57	1.14
DK-4	J ₁ b	Shale	370.00	1.66	0.20	1.16	450.00	69.88	80.12	1.09
DK-5	J ₁ b	Shale	390.00	1.44	0.04	0.19	470.00	13.19	106.25	1.08
DK-6	J ₁ b	Shale	450.00	2.39	0.16	1.22	446.00	51.05	66.95	1.02
DK-7	J ₁ b	Shale	520.00	1.39	0.12	0.35	444.00	25.18	87.05	0.97
DK-8	J ₁ b	Shale	570.00	1.56	0.09	0.97	447.00	62.18	123.08	0.86
DK-9	J ₁ b	Shale	620.00	3.27	0.30	2.69	448.00	82.26	47.09	0.86
DK-10	J ₁ b	Shale	740.00	2.17	0.14	1.23	446.00	56.68	86.18	0.82

Table 2. Rare earth elements of the Beipiao samples, in $\mu\text{g/g}$.

Sample No.	Distance (m)	La	Ce	Pr	Nd	Sm	Eu	Gd	Tb	Dy	Ho	Er	Tm	Yb	Lu	ΣREE	LREE/HREE	δEu	δCe
WL-1	29	60.11	117.66	14.36	54.89	10.72	2.33	7.99	1.13	6.38	1.20	3.35	0.49	3.02	0.42	284.03	10.85	1.19	0.92
WL-2	46	55.41	110.59	13.34	51.55	9.97	2.18	7.08	0.98	5.50	1.01	2.70	0.38	2.55	0.36	263.59	11.82	1.22	0.94
WL-3	94	57.09	113.47	13.88	54.39	10.57	2.23	8.46	1.12	6.52	1.17	3.25	0.46	2.82	0.44	275.85	10.38	1.11	0.93
WL-4	114	67.59	129.06	15.90	62.36	12.13	2.57	9.96	1.37	7.81	1.52	4.30	0.62	4.01	0.59	319.79	9.60	1.10	0.91
WL-5	150	59.23	124.87	14.07	54.21	10.45	2.21	7.94	1.15	6.92	1.34	3.66	0.56	3.61	0.49	290.70	10.32	1.14	1.00
WL-6	250	57.72	123.64	14.59	56.39	11.08	2.08	7.71	1.03	5.92	1.10	2.96	0.44	2.86	0.40	287.92	11.84	1.06	0.98
WL-7	300	52.07	97.74	11.94	45.00	8.12	1.84	6.28	0.86	5.11	0.93	2.59	0.38	2.58	0.35	235.80	11.35	1.21	0.90
WL-8	335	46.68	92.84	11.25	43.44	8.26	2.04	6.90	0.99	5.97	1.17	3.24	0.46	3.13	0.46	226.83	9.16	1.27	0.93
WL-9	380	70.25	148.08	17.41	65.30	11.22	2.11	7.13	0.94	5.44	0.94	2.63	0.37	2.59	0.33	334.73	15.43	1.11	0.98
WL-10	396	36.07	56.87	6.19	19.38	3.24	0.70	2.63	0.51	3.20	0.63	1.77	0.28	1.73	0.22	133.40	11.18	1.13	0.88
DK-1	280	34.21	68.99	4.23	33.09	9.93	1.92	10.83	0.53	9.45	1.60	7.81	0.29	9.62	0.13	192.64	3.78	0.87	1.32
DK-2	310	30.61	85.54	6.96	36.01	6.97	1.73	6.87	0.51	4.22	0.39	1.80	0.24	1.83	0.20	183.87	10.46	1.17	1.35
DK-3	340	27.03	54.34	5.92	31.08	6.33	1.02	6.35	0.43	4.39	0.48	2.31	0.10	2.47	0.12	142.38	7.55	0.76	0.99
DK-4	370	43.87	118.08	9.53	49.21	9.68	2.05	9.74	0.76	6.31	0.70	2.99	0.34	3.19	0.31	256.76	9.55	0.99	1.33
DK-5	390	20.13	61.92	3.86	33.70	10.95	1.77	12.19	0.66	10.46	1.74	8.37	0.23	10.14	0.19	176.32	3.01	0.72	1.62
DK-6	450	18.01	58.88	3.44	30.43	10.19	1.84	11.34	0.61	9.78	1.65	7.94	0.26	9.62	0.15	164.13	2.97	0.80	1.73
DK-7	520	38.08	104.58	8.02	42.91	9.69	1.58	10.62	0.81	7.52	0.97	4.46	0.37	5.43	0.44	235.47	6.69	0.73	1.38
DK-8	570	29.45	67.52	6.49	32.69	6.24	1.30	6.07	0.43	3.80	0.36	1.70	0.16	1.85	0.13	158.17	9.92	0.99	1.13
DK-9	620	32.80	64.19	6.86	35.85	7.37	1.27	7.35	0.52	5.06	0.56	2.63	0.18	2.99	0.19	167.81	7.62	0.81	0.99
DK-10	740	39.39	106.43	9.10	51.75	12.19	2.81	13.23	1.05	8.12	0.89	3.47	0.34	3.35	0.29	252.41	7.21	1.04	1.30

Note: ΣREE : Total concentration of rare earth elements; LREE/HREE: Concentration of light rare earth element/concentration of heavy rare earth element; $\delta\text{Eu} = \text{Eu}/\sqrt{\text{Sm} * \text{Gd}}$ N; $\delta\text{Ce} = \text{Ce}/\sqrt{\text{La} * \text{Pr}}$ N; N: normalized value by PAAS.

4.3. Biomarkers

Fourteen representative samples were selected for GC/MS analyses. The TIC and m/z 191 of WL-1, WL-2 and WL-4 samples indicate that the samples were subjected to secondary alteration (Figure 3a,c), which may include not only thermal alteration but also

degradation. The *n*-alkanes of WL samples were damaged and displayed a significant UCM (unresolved complex mixture) signal, indicating the samples experienced slight biodegradation. The WL samples have Pr/Ph values ranging from 0.62 to 0.92 (averaging 0.76), the DK samples have Pr/Ph values ranging from 1.93 to 3.93 (averaging 2.85). The WL samples display a “V-shaped” C₂₇, C₂₈ and C₂₉ regular sterane relative abundances (Figure 3c). The DK samples are different to the WL samples, which display a “anti-L shape” of sterane. The WL and DK samples distinctly display the difference in the relative abundances of C₁₉, C₂₀ and C₂₃ tricyclic terpanes, regular steranes, gammacerane and 4-methylsteranes (Figure 3b, Table 3), suggesting obvious changes in organic matter origins and depositional environments [56].

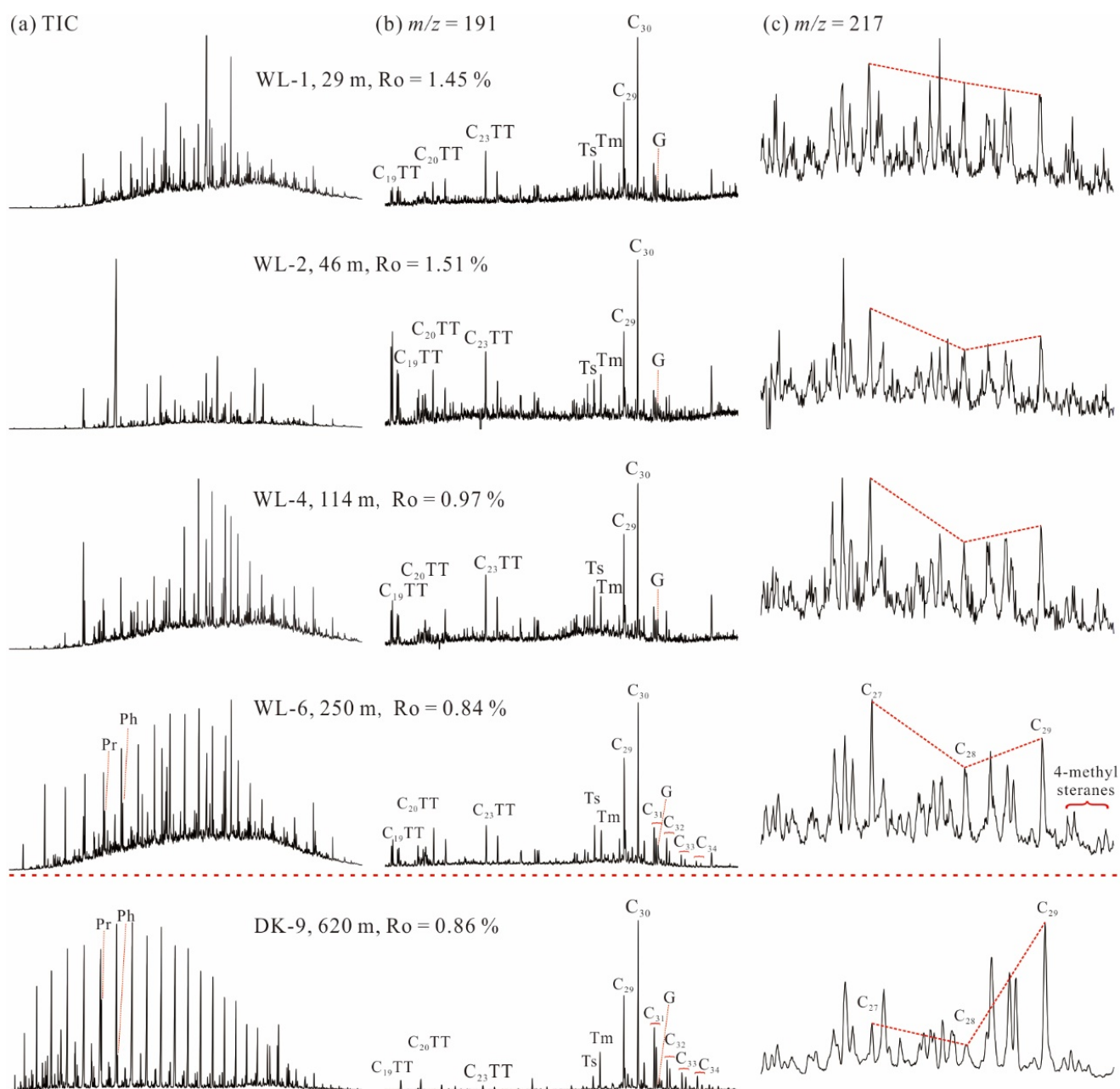


Figure 3. (a) Total ion chromatogram (TIC), (b) $m/z = 191$ and (c) $m/z = 217$ mass chromatograms of saturated hydrocarbon fractions from WL and DK samples.

Table 3. Biomarker parameters of the Beipiao samples.

Sample no.	Fm.	Lithology	Distance (m)	Pr/Ph	20S	$\alpha\beta\beta$	22S	Ts	M/H	C ₂₇ (%)	C ₂₈ (%)	C ₂₉ (%)	C ₁₉₊₂₀ TT (%)	C ₂₁ TT (%)	C ₂₃ TT (%)	C ₁₉ /C ₂₃	C ₂₇ /C ₂₉	S/H	GI	4MSI
WL-1	J ₁ b	Shale	29.00	-	0.49	0.43	0.65	0.54	0.13	35.64	30.55	33.81	16.40	30.39	53.21	0.08	1.05	0.81	0.43	0.23
WL-2	J ₁ b	Shale	46.00	-	0.45	0.40	0.65	0.52	0.14	41.89	27.74	30.37	11.82	34.21	53.97	0.05	1.38	0.89	0.42	0.26
WL-3	J ₁ b	Shale	94.00	0.81	0.43	0.36	0.68	0.55	0.15	38.16	26.58	35.26	28.18	28.51	43.31	0.22	1.08	0.90	0.36	0.28
WL-4	J ₁ b	Shale	114.00	0.62	0.47	0.43	0.66	0.54	0.13	45.26	26.34	28.41	16.35	28.61	55.03	0.09	1.59	1.18	0.48	0.23
WL-5	J ₁ b	Shale	150.00	0.71	0.46	0.42	0.59	0.52	0.13	37.82	29.60	32.58	17.15	28.38	54.47	0.07	1.16	0.91	0.50	0.22
WL-6	J ₁ b	Shale	250.00	0.79	0.48	0.42	0.65	0.54	0.13	35.55	31.60	32.85	19.42	32.69	47.89	0.12	1.08	0.80	0.38	0.29
WL-7	J ₁ b	Shale	300.00	0.92	0.50	0.43	0.60	0.51	0.13	38.89	30.38	30.74	21.29	28.38	50.33	0.10	1.27	0.73	0.46	0.26
WL-8	J ₁ b	Shale	335.00	0.87	0.45	0.40	0.68	0.51	0.13	39.83	28.71	31.46	17.00	30.62	52.38	0.16	1.27	0.92	0.38	0.26
WL-9	J ₁ b	Shale	380.00	0.70	0.48	0.41	0.71	0.53	0.12	39.04	30.79	30.17	20.50	30.53	48.96	0.09	1.29	1.18	0.36	0.25
WL-10	J ₁ b	Shale	396.00	0.63	0.48	0.40	0.66	0.53	0.14	33.83	32.58	33.59	14.69	33.34	51.97	0.07	1.01	0.80	0.74	0.16
DK-4	J ₁ b	Shale	370.00	2.95	0.50	0.52	0.59	0.69	0.12	26.55	27.30	46.15	56.13	20.55	23.32	0.95	0.73	0.49	0.16	0.05
DK-5	J ₁ b	Shale	390.00	2.57	0.48	0.43	0.60	0.40	0.13	26.91	22.27	50.82	63.59	17.62	18.79	1.65	0.89	0.16	0.08	0.04
DK-9	J ₁ b	Shale	620.00	3.93	0.45	0.38	0.59	0.26	0.13	25.48	20.11	54.41	68.66	16.48	14.87	2.31	0.66	0.12	0.05	0.04
DK-10	J ₁ b	Shale	740.00	1.93	0.52	0.49	0.61	0.89	0.09	32.29	25.12	42.59	63.04	16.97	19.98	1.02	1.01	0.70	0.46	0.04

Note: Pr/Ph: pristane/phytane; 20S: 20S/(20S + 20R) ratio for C₂₉- $\alpha\alpha\alpha$ steranes; $\alpha\beta\beta$: $\alpha\beta\beta/(\alpha\alpha\alpha + \alpha\beta\beta)$ ratio for C₂₉-steranes; 22S: 22S/(22S + 22R) ratio for C₃₂ hopanes; Ts/Tm: 18 α (H)-/(17 α (H) + 18 α (H))-trisnorhopane ratio; M/H: C₃₀ moretane/C₃₀ hopane; C₂₇, C₂₈, C₂₉: Relative abundance of C₂₇, C₂₈, C₂₉ - $\alpha\alpha\alpha$ 20R among C₂₇-C₂₉ - $\alpha\alpha\alpha$ 20R steranes; C₁₉₊₂₀TT, C₂₁TT, C₂₃TT: Relative abundance of C₁₉₊₂₀, C₂₁, C₂₃ tricyclic terpane; C₁₉/C₂₃ = C₁₉ tricyclic terpane/C₂₃ tricyclic terpane; C₂₇/C₂₉ = C₂₇ sterane/C₂₉ sterane; S/H = steranes/hopanes; GI = gammacerane index (gammacerane/C₃₁ hopane); 4MSI = 4-methylsterane index (4-methylsterane/C₂₉ sterane). “-” represents no data or not determined.

GC/MS of the saturated hydrocarbons show a noticeable loss of *n*-alkanes adjacent to the magmatic activity, as well as a shift in the carbon number distribution to a predominance of the shorter chain-length homologues (Figure 3a). The thermal cracking of hopanes in the WL samples with higher maturity, the content of C₃₃ and C₃₄ hopanes are lower. The ratios of 22S/(22R + 22R) for the C₃₂ hopanes are considered as excellent indicators of thermal maturation [56]. The 22S/(22R + 22R) values of WL samples are distinctly higher than that of DK samples. Other maturity indicators reach equilibrium or are even reversed due to their high maturity (Table 3). The above phenomena of WL samples are typical features of thermal stress closest to the granite porphyry dike [22,57].

5. Discussion

5.1. Evidence of Magmatic-Hydrothermal Activities

Previous studies have suggested that hydrothermal activity is often closely related to the intrusion or eruption of magma [24–26]. According to the U-Pb dating data and previous studies [50,51], it is indicated that the diorite porphyry dike might intrude during the deposition of the dark coal-bearing strata in the Beipiao Formation. The Ni-Co-Zn ternary diagram [58] shows that all the WL samples plot in the hydrothermal deposition area (Figure 4 and Table 4), indicating that hydrothermal activity occurred during the deposition of the WL samples. Rare earth elements are often used as tracers of hydrothermal activity [59–61]. The WL samples generally display the higher total rare earth content and higher LREE/HREE ratios, with significant positive Eu anomalies (averaging 1.15) and negative Ce anomalies (averaging 0.94). On the contrary, the DK samples generally display the lower total rare earth content and lower LREE/HREE ratios, with significant negative Eu anomalies (averaging 0.89) and positive Ce anomalies (averaging 1.31). The positive Eu anomalies and negative Ce anomalies indicate that the formation of WL samples is associated with hydrothermal activity (Table 2 and Figure 5) [29,59–62].

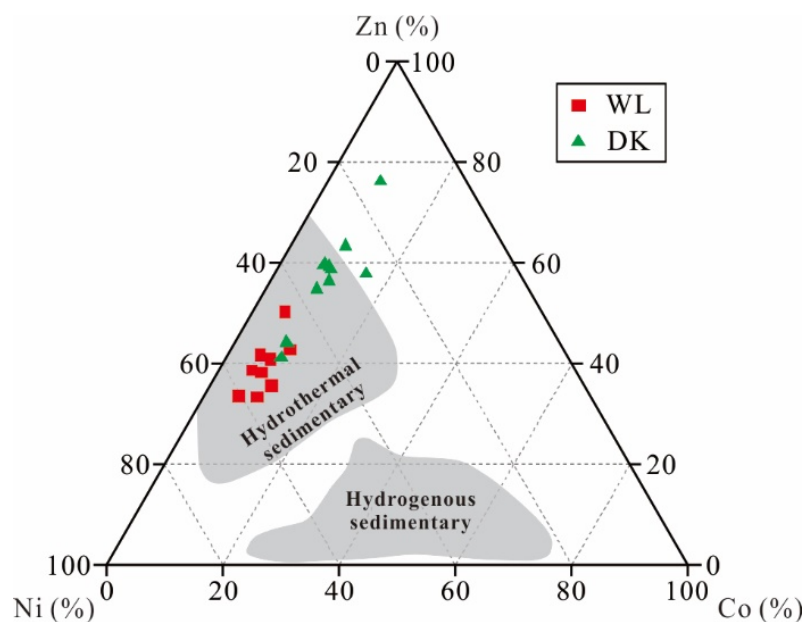
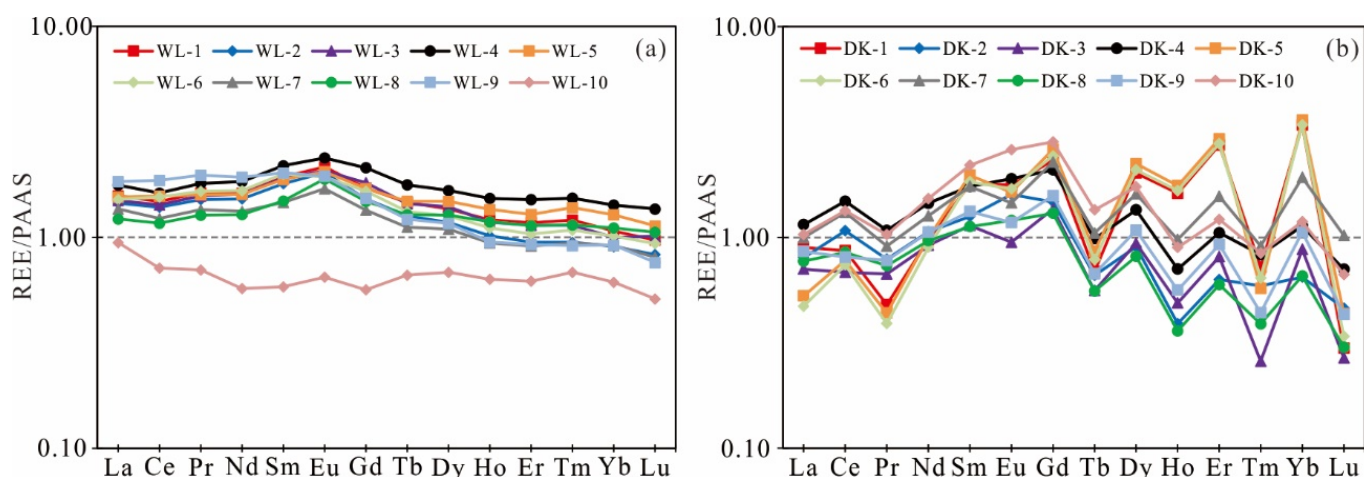


Figure 4. Ternary diagrams showing the relative distribution of Ni-Co-Zn [58].

Table 4. Trace elements of the Beipiao samples, in $\mu\text{g/g}$.

Sample No.	Fm.	Lithology	Co	Ni	Zn
WL-1	J ₁ b	Shale	21.96	150.22	118.74
WL-2	J ₁ b	Shale	20.99	145.05	115.84
WL-3	J ₁ b	Shale	26.81	171.63	99.55
WL-4	J ₁ b	Shale	21.40	160.33	112.85
WL-5	J ₁ b	Shale	24.39	115.97	105.27
WL-6	J ₁ b	Shale	27.88	145.31	96.17
WL-7	J ₁ b	Shale	10.05	100.50	79.33
WL-8	J ₁ b	Shale	9.92	105.82	58.54
WL-9	J ₁ b	Shale	9.44	96.46	67.21
WL-10	J ₁ b	Shale	4.16	35.34	40.03
DK-1	J ₁ b	Shale	24.85	70.87	165.80
DK-2	J ₁ b	Shale	31.27	53.41	116.73
DK-3	J ₁ b	Shale	18.74	69.26	127.86
DK-4	J ₁ b	Shale	25.41	110.08	200.36
DK-5	J ₁ b	Shale	26.71	141.51	133.05
DK-6	J ₁ b	Shale	37.37	197.21	163.98
DK-7	J ₁ b	Shale	35.41	58.50	302.34
DK-8	J ₁ b	Shale	21.82	74.29	135.88
DK-9	J ₁ b	Shale	24.53	104.40	156.69
DK-10	J ₁ b	Shale	33.02	110.92	185.75

**Figure 5.** Distribution pattern of rare earth elements in the (a) WL samples and (b) DK samples.

5.2. Influence of Magmatism on Organic Matter Abundance

S_2 and TOC are commonly combined to evaluate the hydrocarbon-generating potential of source rock, and better petroleum source rocks are characterized by relatively higher S_2 and TOC values [63–65]. According to the evaluation criteria of source rock [52], the TOC values suggest that most of the WL and DK samples are good to very good and fair to good source rocks, respectively (Figure 6). However, both WL and DK samples have a relatively low amount of free hydrocarbons (S_1) and hydrocarbons generated by pyrolytic degradation of the kerogen in the rock (S_2), indicating that the remaining hydrocarbon potential for the samples is low (Table 1), which maybe related to the higher maturity.

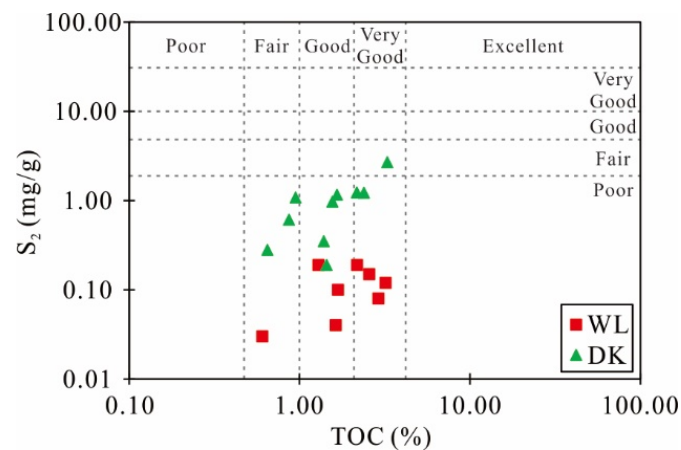


Figure 6. Cross-plot of S_2 and TOC for determining the quality of source rocks.

The relationship between the TOC and distance from the granite porphyry dike shows a progressive decrease in TOC toward the magmatic intrusion, before undergoing a reversal (Figure 7a). A significant decrease in TOC values in source rocks heated by magmatic intrusions is common in other examples due to the destructive effect on the organic matter by the intrusive heating, as in the DK samples [9,66,67]. By contrast, the TOC values, in which WL samples increase with the distance to the granite porphyry dike, decrease. This phenomenon may be related to the fact that the magmatic-hydrothermal activities in the Wolong area is conducive to the enrichment and preservation of organic matter. According to the relationship between the Rock-Eval pyrolysis parameters and the distance to the granite porphyry dike, when the distance from the source rock to the granite porphyry dike decreases, the hydrocarbon generation potential and HI decrease gradually (Figure 7b,c). The phenomenon is consistent with previous reports [18,22]. Rock-Eval results support the assumption of the high thermal stress and destruction of hydrocarbons within the thermal aureole, especially for WL samples, which are closer to the granite porphyry dike.

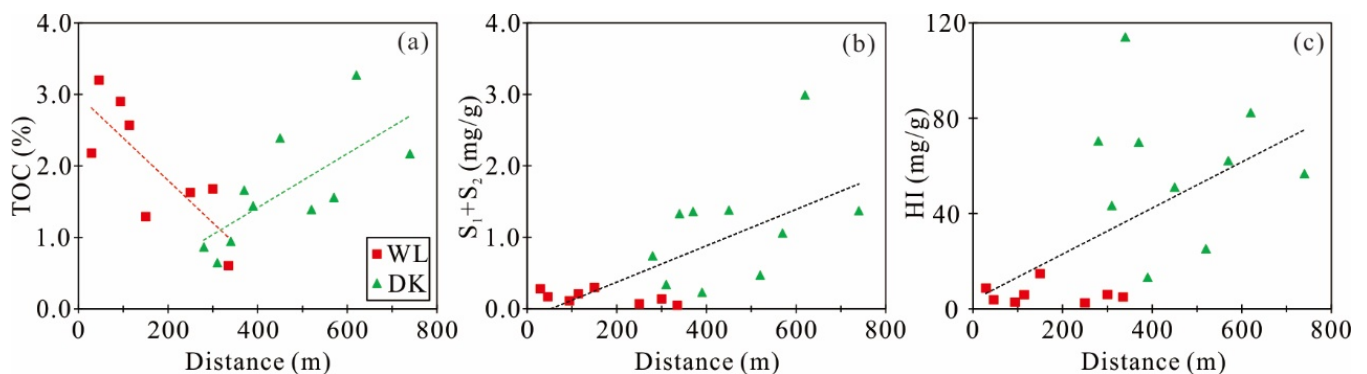


Figure 7. Cross plot of TOC (a), $S_1 + S_2$ (b) and HI (c) versus distance from the granite porphyry dike.

5.3. Influence of Magmatism on Hydrocarbon Evolution Stage of Source Rocks

The heat source associated with magmatic intrusion had a significant effect on the transformation of organic matter in the organic-rich host rock and could also promote the hydrocarbon generation process. In most cases studied, the thermal effect of igneous bodies intruded into sedimentary rocks is expected to be one to two times the thickness of the igneous body [9,22,68,69]. The Ro values suggest that both WL (Ro = 1.17%) and DK (Ro = 1.01%) samples have entered the oil-generating stage, and WL samples were influenced by the intrusive body with higher maturity (Table 1). According to the relationship between the maturity and distance from the granite porphyry dike, the maturity of the

samples with a distance of less than 100 m (the average Ro is 1.46%) is significantly higher than others (Figure 8). When the distance between the sample and the granite porphyry dike is more than 100 m, the maturity (the average Ro is 1.00%) is gradually stable and decreases to the regional background values [37]. Therefore, the baking of the intrusive body significantly affected the maturity of WL samples, but had little influence on DK samples. Thermal maturation effects of igneous bodies on source rocks have been well described and show different ranges of maturity that vary with the number of sills, spacing, thickness, emplacement time, temperature of magma, length and distances between the igneous bodies and host rock [6,17,18,69,70]. However, the causes of the heat effect are not fully understood at this stage, and further research is required.

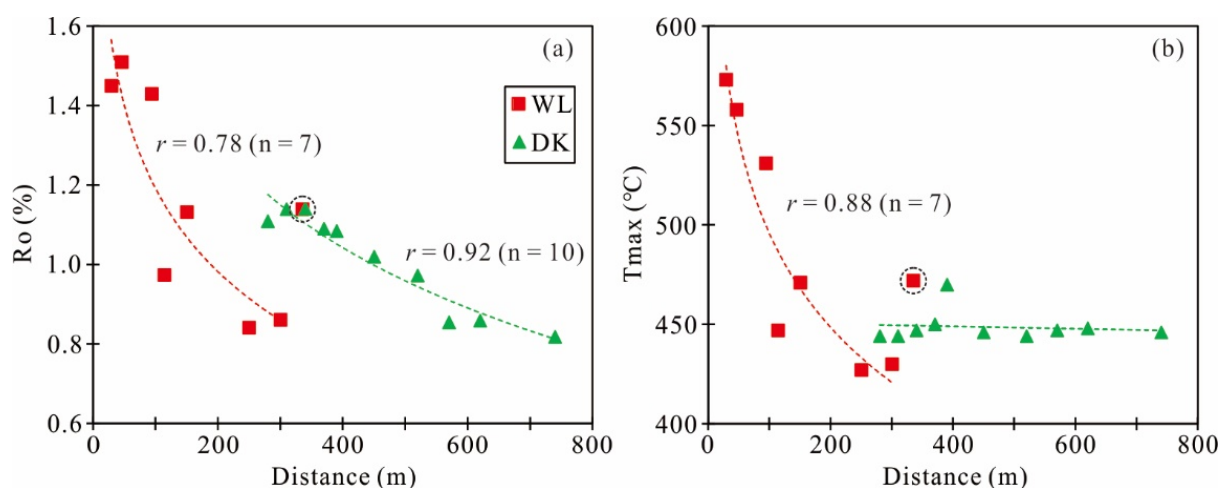


Figure 8. Cross plot of Ro (a) and Tmax (b) versus distance from the granite porphyry dike.

5.4. Influence of Magmatic-Hydrothermal Activities on the Sedimentary Environment and Organic Matter Input

The tricyclic terpene results are further used for the evaluation of the organic matter origin and source input [71–75]. C_{19} and C_{20} tricyclic terpenes are mainly derived from terrestrial higher plants [76], while C_{23} tricyclic terpenes are mainly derived from algae [77]. Among the samples analyzed in this study, the WL samples generally display the lower C_{19}/C_{23} TT ratios (averaging 0.10), indicating a relatively high contribution from algae sources. The DK samples display high C_{19}/C_{23} TT values (averaging 1.48), suggesting relatively high terrestrial organic matter input (Figure 9a).

Higher plants and algae are the source of sterols, which are believed to be the origin of steranes [78]. It is generally believed that C_{27} steranes derive mainly from phytoplankton and metazoa, and C_{28} steranes are associated with specific phytoplankton types (e.g., diatoms) [79,80] that contain chlorophyll-c [81], whereas C_{29} steranes mainly originate from terrigenous higher plants [78,82]. The regular steranes' (C_{27} , C_{28} , and C_{29}) relative proportions can vary dramatically between samples and are influenced by the type of OM source [78,82]. C_{27} - C_{28} - C_{29} $\alpha\alpha\alpha$ -20R regular sterane ternary plot shows that the organic matter source of the WL sample is mainly aquatic organisms, while that of the DK sample has more terrigenous organic matter input (Figure 10a). In addition, the value of the C_{27}/C_{29} steranes show similar characteristics (Figure 9a).

The ratios of steranes to hopanes is used to determine the relative contributions of eukaryotic (mainly algae and higher plants) versus prokaryotic (bacterial) organic matter of the source rocks [56,83,84]. The Steranes/Hopanes ratios increase as the abundance of C_{27} sterane increase and decrease as the abundance of C_{29} sterane increase (Figure 9c), indicating that high Steranes/Hopanes ratios were caused by the contribution from phytoplankton rather than that of terrigenous higher plants [81]. The relatively high Steranes/Hopanes ratios of WL samples (averaging 0.91) indicate a relatively higher contribution of phytoplankton, whereas the relatively low Steranes/Hopanes ratios of DK samples (averaging

0.37) suggest higher terrigenous plant input (Figure 9b), which is consistent with the tricyclic terpanes result.

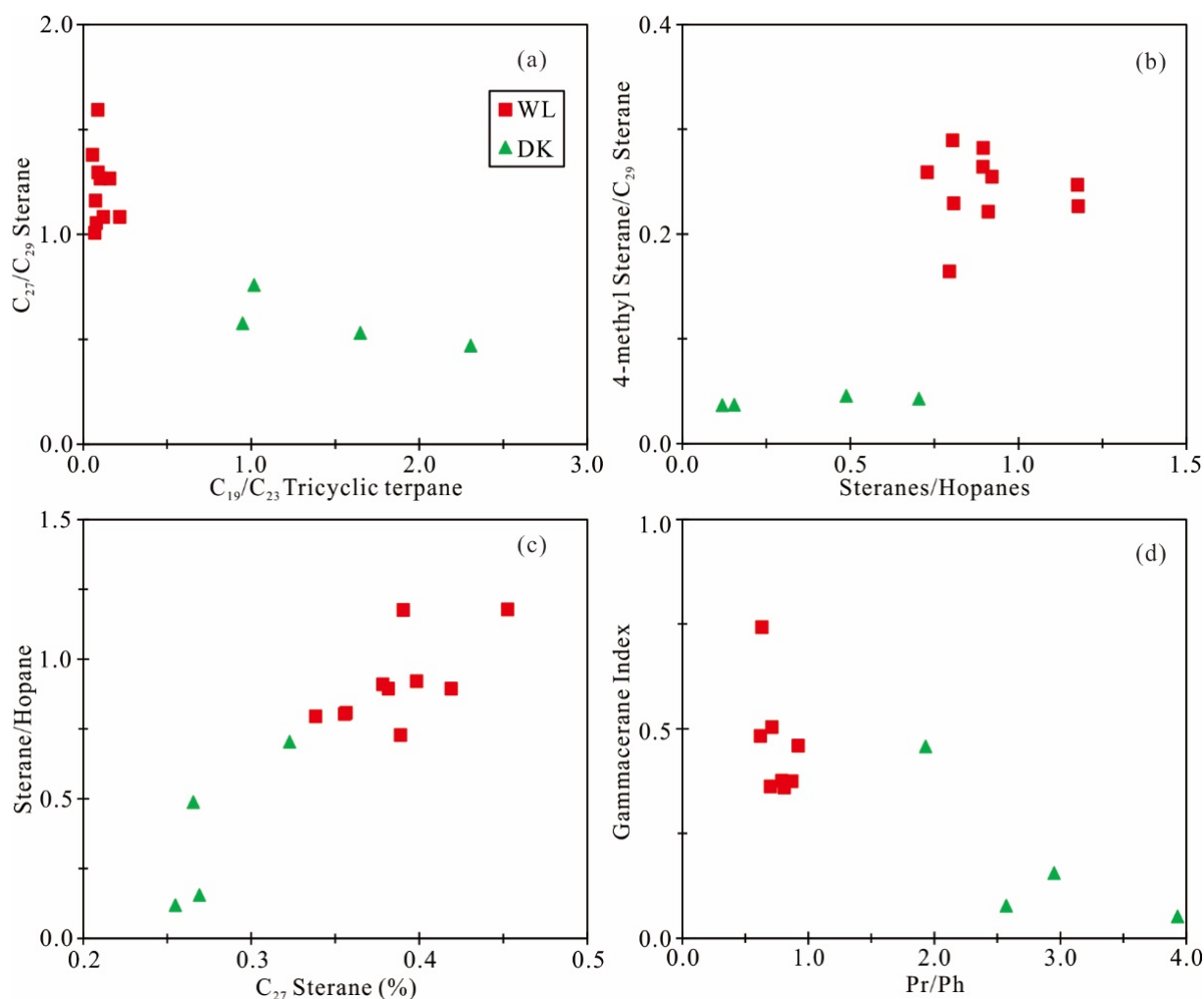


Figure 9. Correlation between various biomarker parameters reflecting organic matter input (a–c) and depositional environments (d) for the WL and DK samples.

A high abundance of 4-methyl steranes is associated with the input of dinoflagellates [85,86]. These dinoflagellates mostly exist in marine sedimentary rocks with immature organic matter or in lacustrine sedimentary rocks with high water salinity due to transgression [87,88]. The higher 4-methyl steranes/ C_{29} steranes ratios of WL samples may suggest a higher input of saltwater algal organic matter (Figure 9b). By contrast, the DK samples display relatively low 4-methyl steranes/ C_{29} steranes ratios, suggesting limited contributions from the algae.

A ternary plot on the relative abundance of C_{19+20} – C_{21} – C_{23} tricyclic terpene has been successfully applied to differentiate the depositional environments of the source rocks and crude oils [89]. The diagram shows that the depositional environment of the WL samples is mainly saline lacustrine, while that of the DK samples is mainly swamp (Figure 10b). Biomarkers are also useful proxies for paleoenvironmental reconstruction. Pristane (Pr) and phytane (Ph) are generated from phytol [90], which can be converted to Ph and Pr under reducing environments and oxic conditions, respectively [90]. Therefore, the Pr/Ph values correlate with the redox condition during sediment deposition. Generally, Pr/Ph values less than one suggest suboxic-anoxic conditions, whereas Pr/Ph values greater than one are associated with oxic conditions in sediments [90]. The Pr/Ph value of WL samples is significantly lower than that of DK samples (Figure 9d). Although the origin of

gammacerane is unclear, it can be used to characterize stratified water in the sedimentary environment of source rocks, which results in high salinity and/or anoxic conditions in bottom waters [91,92]. Therefore, the gammacerane index is frequently used as a specific biomarker for water-column stratification and/or hypersaline conditions [92]. Overall, the WL samples had higher gammacerane index values than DK samples (Figure 9d). WL samples generally show the homohopane tail-raising phenomenon (Figure 3), indicating the original sedimentary environment of reducing reductive salt water [56]. The above biomarkers reveal that WL and DK samples were formed in anoxic saline and aerobic freshwater sedimentary environments, respectively.

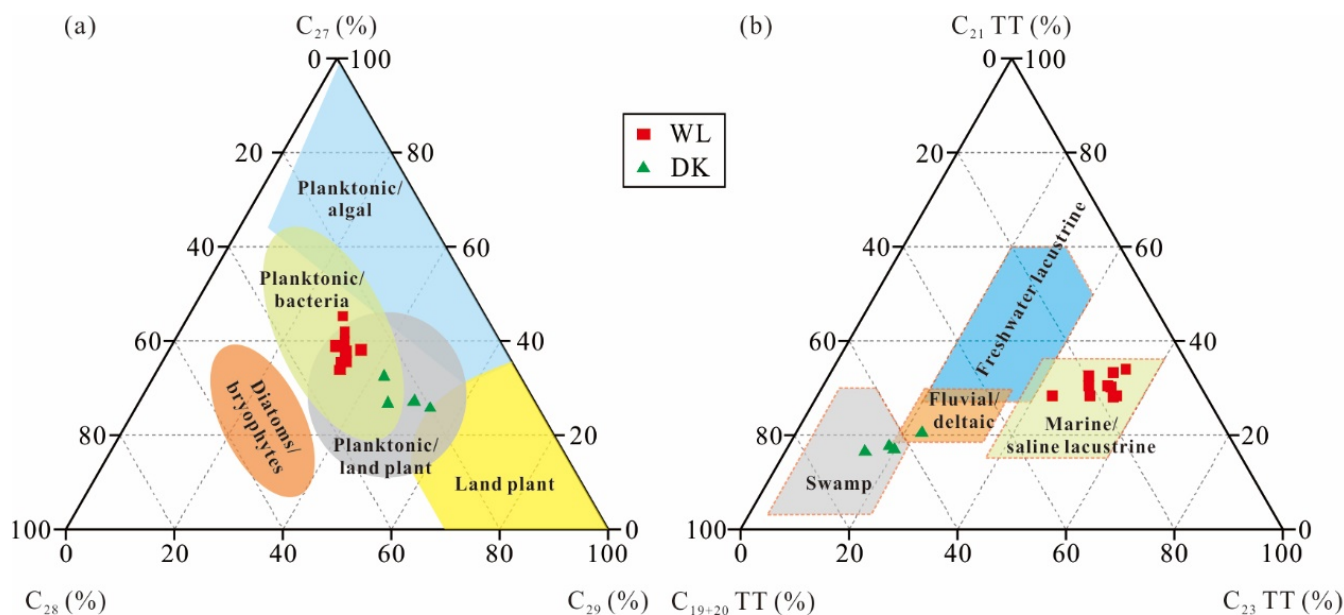


Figure 10. Ternary diagrams showing the relative distribution of (a) C_{27} - C_{28} - C_{29} -sterane [86] and (b) C_{19+20} - C_{21} - C_{23} -tricyclic terpane [89].

6. Conclusions

- (1) The hydrothermal indicator discrimination diagram (Zn-Ni-Co triangular plot) and rare earth element anomalies (δEu and δCe) indicate hydrothermal activity occurred during the deposition of the WL samples, but not for the DK samples.
- (2) The TOC values indicate that the organic matter abundance of the WL samples was higher than that of the DK samples.
- (3) The WL samples were influenced by the magmatic intrusion with higher maturity, demonstrating the magmatic-hydrothermal activities promoted a hydrocarbon generation process.
- (4) The magmatic-hydrothermal activities brought abundant nutrients to the lake basin, increased the salinity of water and promoted the formation of a water reducing environment, resulting in the formation of organic-rich source rocks.

Author Contributions: Conceptualization, S.D. and S.L.; methodology, S.D. and S.L.; software, S.D.; investigation, S.D. and S.L.; resources, S.S.; data curation, S.D.; writing—original draft preparation, S.D.; writing—review and editing, S.D. and S.L.; visualization, S.D. and S.L.; supervision, S.L.; project administration, S.S. and Y.L.; linguistic revisions, Z.H. and M.Q. All authors have read and agreed to the published version of the manuscript.

Funding: This research was funded by National Natural Science of China, Grant No. 41790451; China Geological Survey oil and gas survey program, Grant No. DD20221664.

Institutional Review Board Statement: Not applicable.

Informed Consent Statement: Not applicable.

Data Availability Statement: Not applicable.

Acknowledgments: The authors would like to thank anonymous reviewers for their constructive comments and suggestions which significantly improve the quality of this manuscript.

Conflicts of Interest: The authors declare no conflict of interest.

References

1. Monreal, F.R.; Villar, H.; Baudino, R.; Delpino, D.; Zencich, S. Modeling an atypical petroleum system: A case study of hydrocarbon generation, migration and accumulation related to igneous intrusions in the Neuquen Basin, Argentina. *Mar. Pet. Geol.* **2009**, *26*, 590–605. [[CrossRef](#)]
2. Jackson, C.A.-L.; Schofield, N.; Golenkov, B. Geometry and controls on the development of igneous sill-related forced folds: A 2-D seismic reflection case study from offshore southern Australia. *GSA Bull.* **2013**, *125*, 1874–1890. [[CrossRef](#)]
3. Fjeldskaar, W.; Helset, H.M.; Johansen, H.; Grunnaleite, I.; Horstad, I. Thermal modelling of magmatic intrusions in the Gjallar Ridge, Norwegian Sea: Implications for vitrinite reflectance and hydrocarbon maturation. *Basin Res.* **2008**, *20*, 143–159. [[CrossRef](#)]
4. Aarnes, I.; Planke, S.; Trulsvik, M.; Svensen, H. Contact metamorphism and thermogenic gas generation in the Vøring and Møre basins, offshore Norway, during the Paleocene–Eocene thermal maximum. *J. Geol. Soc.* **2015**, *172*, 588–598. [[CrossRef](#)]
5. Svensen, H.; Planke, S.; Polozov, A.G.; Schmidbauer, N.; Corfu, F.; Podladchikov, Y.Y.; Jamtveit, B. Siberian gas venting and the end-Permian environmental crisis. *Earth Planet. Sci. Lett.* **2009**, *277*, 490–500. [[CrossRef](#)]
6. Aarnes, I.; Svensen, H.; Connolly, J.A.; Podladchikov, Y.Y. How contact metamorphism can trigger global climate changes: Modeling gas generation around igneous sills in sedimentary basins. *Geochim. Cosmochim. Acta* **2010**, *74*, 7179–7195. [[CrossRef](#)]
7. Othman, R.; Arouri, K.R.; Ward, C.R.; McKirdy, D.M. Oil generation by igneous intrusions in the northern Gunnedah Basin, Australia. *Org. Geochem.* **2001**, *32*, 1219–1232. [[CrossRef](#)]
8. Jones, S.; Wielens, H.; Williamson, M.-C.; Zentilli, M. Impact of magmatism on petroleum systems in the sverdrup basin, canadian arctic islands, nunavut: A numerical modelling study. *J. Pet. Geol.* **2007**, *30*, 237–256. [[CrossRef](#)]
9. Cooper, J.R.; Crelling, J.C.; Rimmer, S.M.; Whittington, A.G. Coal metamorphism by igneous intrusion in the Raton Basin, CO and NM: Implications for generation of volatiles. *Int. J. Coal Geol.* **2007**, *71*, 15–27. [[CrossRef](#)]
10. Delpino, D.H.; Bermúdez, A.M. Petroleum systems including unconventional reservoirs in intrusive igneous rocks (sills and laccoliths). *Lead. Edge* **2009**, *28*, 804–811. [[CrossRef](#)]
11. Karvelas, A.; Magee, C.; Shtukert, O.; Schenk, O.; Devine, T. Understanding Magmatic History and its Implications upon Petroleum Systems of the NE Rockall Basin. In Proceedings of the 77th EAGE Conference and Exhibition 2015. European Association of Geoscientists & Engineers, Madrid, Spain, 1–4 June 2015. [[CrossRef](#)]
12. Svensen, H.; Planke, S.; Malthe-Sørenssen, A.; Jamtveit, B.; Myklebust, R.; Eidem, T.R.; Rey, S.S. Release of methane from a volcanic basin as a mechanism for initial Eocene global warming. *Nature* **2004**, *429*, 542–545. [[CrossRef](#)]
13. Cartwright, J.; Huuse, M.; Aplin, A. Seal bypass systems. *AAPG Bull.* **2007**, *91*, 1141–1166. [[CrossRef](#)]
14. Rateau, R.; Schofield, N.; Smith, M. The potential role of igneous intrusions on hydrocarbon migration, West of Shetland. *Pet. Geosci.* **2013**, *19*, 259–272. [[CrossRef](#)]
15. Haug, T.; Galland, O.; Souloumiac, P.; Souche, A.; Guldstrand, F.; Schmiedel, T. Inelastic damage as a mechanical precursor for the emplacement of saucer-shaped intrusions. *Geology* **2017**, *45*, 1099–1102. [[CrossRef](#)]
16. Schmiedel, T.; Kjøberg, S.; Planke, S.; Magee, C.; Galland, O.; Schofield, N.; Jackson, C.A.-L.; Jerram, D.A. Mechanisms of overburden deformation associated with the emplacement of the Tulipan sill, mid-Norwegian margin. *Interpretation* **2017**, *5*, SK23–SK38. [[CrossRef](#)]
17. Zalán, P.V.; Wolff, S.; Conceição, J.C.J.; Marques, A.; Astolfi, M.A.M.; Vieira, I.S.; Appi, V.T.; Zannotto, O.A. Bacia Do Paraná. In *Origem e Evolução de Bacias Sedimentares*; Raja Gabiglia, G.P., Milani, E.J., Eds.; Petrobras: Rio de Janeiro, Brazil, 1990; pp. 681–708.
18. Spacapan, J.; Palma, J.; Galland, O.; Manceda, R.; Rocha, E.; D’Odorico, A.; Leanza, H. Thermal impact of igneous sill-complexes on organic-rich formations and implications for petroleum systems: A case study in the northern Neuquén Basin, Argentina. *Mar. Pet. Geol.* **2018**, *91*, 519–531. [[CrossRef](#)]
19. Filho, A.T.; Mizusaki, A.M.P.; Antonioli, L. Magmatism and petroleum exploration in the Brazilian Paleozoic basins. *Mar. Pet. Geol.* **2008**, *25*, 143–151. [[CrossRef](#)]
20. Santos, R.V.; Dantas, E.L.; de Oliveira, C.G.; de Alvarenga, C.J.S.; dos Anjos, C.W.D.; Guimarães, E.M.; Oliveira, F.B. Geochemical and thermal effects of a basic sill on black shales and limestones of the Permian Irati Formation. *J. S. Am. Earth Sci.* **2009**, *28*, 14–24. [[CrossRef](#)]
21. Annen, C. Implications of incremental emplacement of magma bodies for magma differentiation, thermal aureole dimensions and plutonism–volcanism relationships. *Tectonophysics* **2011**, *500*, 3–10. [[CrossRef](#)]
22. Agirrezabala, L.M.; Permanyer, A.; Suárez-Ruiz, I.; Dorransoro, C. Contact metamorphism of organic-rich mudstones and carbon release around a magmatic sill in the Basque-Cantabrian Basin, western Pyrenees. *Org. Geochem.* **2014**, *69*, 26–35. [[CrossRef](#)]
23. Sydnes, M.; Fjeldskaar, W.; Løtveit, I.F.; Grunnaleite, I.; Cardozo, N. The importance of sill thickness and timing of sill emplacement on hydrocarbon maturation. *Mar. Pet. Geol.* **2018**, *89*, 500–514. [[CrossRef](#)]

24. Skinner, B. The Many Origins of Hydrothermal Mineral Deposits. In *Geochemistry of Hydrothermal Ore Deposits*, 2nd ed.; Barnes, H.L., Ed.; John Wiley & Sons: New York, NY, USA, 1979; pp. 3–21.
25. Qi, H.; Hu, R.; Su, W.; Qi, L.; Feng, J. Continental hydrothermal sedimentary siliceous rock and genesis of superlarge germanium (Ge) deposit hosted in coal: A study from the Lincang Ge deposit, Yunnan, China. *Sci. China Ser. D Earth Sci.* **2004**, *47*, 973–984. [[CrossRef](#)]
26. Zhang, Y.; Horsfield, B.; Hou, D.; Noah, M.; Yang, S. Impact of hydrothermal activity on organic matter quantity and quality during deposition in the Permian Dalong Formation, Southern China. *Mar. Pet. Geol.* **2019**, *110*, 901–911. [[CrossRef](#)]
27. Sun, X.; Chen, J.; Zheng, J.; Liu, W. Geochemical characteristics of organic matter-rich sedimentary strata in Lower Cambrian, Tarim Basin and its origins. *Acta Sedimentol. Sin.* **2004**, *22*, 548–552. (In Chinese with English Abstract)
28. Liu, J.; Liu, Q.; Zhu, D.; Meng, Q.; Liu, W.; Qiu, D.; Huang, Z. The role of deep fluid in the formation of organic-rich source rocks☆. *J. Nat. Gas Geosci.* **2018**, *3*, 171–180. [[CrossRef](#)]
29. Liu, Q.; Zhu, D.; Jin, Z.; Meng, Q.; Li, S. Influence of volcanic activities on redox chemistry changes linked to the enhancement of the ancient Sinian source rocks in the Yangtze craton. *Precambrian Res.* **2019**, *327*, 1–13. [[CrossRef](#)]
30. Gao, P.; He, Z.; Li, S.; Lash, G.G.; Li, B.; Huang, B.; Yan, D. Volcanic and hydrothermal activities recorded in phosphate nodules from the Lower Cambrian Niutitang Formation black shales in South China. *Palaeogeogr. Palaeoclim. Palaeoecol.* **2018**, *505*, 381–397. [[CrossRef](#)]
31. Zhang, W.; Yang, H.; Xie, L.; Yang, Y. Lake-bottom hydrothermal activity and their influences on the high-quality source rock development: A case from Chang 7 source rocks in Ordos Basin, China. *Pet. Explor. Dev.* **2010**, *37*, 424–429. (In Chinese with English Abstract)
32. Wu, F.Y.; Sun, D.Y.; Ge, W.C.; Zhang, Y.B.; Grant, M.L.; Wilde, S.A.; Jahn, B.M. Geochronology of the Phanerozoic granitoids in northeastern China. *J. Asian Earth Sci.* **2011**, *41*, 1–30. [[CrossRef](#)]
33. Zhen, Z.; Li, Y.F.; Gao, X.Y.; Sun, S.L.; Zhou, T.S. Characteristics of sedimentary facies and organic matter of Lower Jurassic Beipiao Formation of Well SZK01 in Jinyang Basin. *Glob. Geol.* **2016**, *35*, 207–215. (In Chinese with English Abstract)
34. Sun, S.L.; Li, Y.F.; Gao, X.Y.; Zhou, T.S.; Zhang, T.; Wang, S.H. An analysis of the genesis and geochemical characteristics of shale gas in Lower Jurassic Beipiao Formation in Jinyang Basin. *Geol. Bull. China* **2017**, *36*, 575–581. (In Chinese with English Abstract)
35. Sun, S.L.; Li, Y.F.; Chen, S.W.; Gao, X.Y.; Sun, Q.S.; Zhang, K.; Zhou, T.S. Depositional environment and organic geochemical characteristics of source rocks of Beipiao Formation in Jinyang Basin. *Glob. Geol.* **2017**, *36*, 889–902. (In Chinese with English Abstract)
36. Sun, S.L.; Zhang, T.; Liu, M.; Li, Y.F.; Chen, S.W.; Zhang, J.; Tang, Y.J.; Sun, Q.S. Sedimentary environment and genesis of source rocks of Beipiao Formation in Jinyang Basin, Western Liaoning. *J. Northeast. Pet. Univ.* **2019**, *43*, 1–12. (In Chinese with English Abstract)
37. Sun, S.; Zhang, T.; Li, Y.; Chen, S.; Sun, Q. Effects of igneous intrusions on source rock in the early diagenetic stage: A case study on Beipiao Formation in Jinyang Basin, Northeast China. *Open Geosci.* **2020**, *12*, 990–1002. [[CrossRef](#)]
38. Mou, H.S.; Xue, X.Y.; Jiang, Z.X. Exploration status and prospect of shale oil and gas in the Mesozoic Basins, Eastern Yanshan Orogenic Belt. *Earth Sci. Front.* **2022**, 1–14, *in press*. (In Chinese with English Abstract)
39. Liu, X. Some viewpoints on Yanshan Movement in Eastern China. *Geol. Rev.* **1982**, *28*, 428–438. (In Chinese with English Abstract)
40. Zhou, L.D.; Zhao, M.P. Study on evolution history of the fault zone on the west edge of Jinlingsi-Yangshan Basin in west Liaoning. *Liaoning Geol.* **1999**, *16*, 249–254. (In Chinese with English Abstract)
41. Wang, G.H.; Zhang, C.H.; Wang, S.G. Tectonic framework of Western Liaoning Province and its evolution during Mesozoic. *Geoscience* **2001**, *15*, 1–7. (In Chinese with English Abstract)
42. Li, Z.; Liu, S.; Zhang, J.; Wang, Q. Typical basin-fill sequences and basin migration in Yanshan, North China. *Sci. China Ser. D: Earth Sci.* **2004**, *47*, 181–192. [[CrossRef](#)]
43. Yan, Y.; Lin, G.; Li, Z. Characteristics of the Jurassic filling sequence and the indication of tectonic evolution of Beipiao basin, western Liaoning. *J. Strat.* **2002**, *26*, 151–155. (In Chinese with English Abstract)
44. Liu, S.; Zhang, J.; Hong, S.; Ritts, B.D. Early Mesozoic Basin Development and Its Response to Thrusting in the Yanshan Fold-and-Thrust Belt, China. *Int. Geol. Rev.* **2007**, *49*, 1025–1049. [[CrossRef](#)]
45. Liu, S.; Li, Z.; Zhang, J. Mesozoic basin evolution and tectonic mechanism in Yanshan, China. *Sci. China Ser. D Earth Sci.* **2004**, *47*, 24–38. [[CrossRef](#)]
46. Li, Y.; Chen, S. A new discovery of oil and gas in Jinyang Basin, western Liaoning province. *Geol. Bull. China* **2014**, *33*, 1463–1464. (In Chinese with English Abstract)
47. Zhang, T.; Li, Y.F.; Sun, S.L.; Gao, X.Y.; Zhou, T.S.; Sun, P. Saturated hydrocarbon geochemical characteristics of the oil sand from YD1 well in Jinyang Basin and its significance for oil and gas exploration. *Geol. Bull. China* **2017**, *36*, 582–590. (In Chinese with English Abstract)
48. Liu, M.; Chen, J.S.; Sun, S.L.; Li, B.; Yang, F.; Zhang, T.; Wang, Y.; Wu, Z. Stratigraphic sequence and characteristics of depositional system of the Beipiao Formation in the Beipiao (Jin-Yang) basin, western Liaoning. *Geol. Bull. China* **2018**, *37*, 1755–1759. (In Chinese with English Abstract)
49. Liu, M.; Zhang, Y.J.; Sun, S.L.; Chen, J.S.; Li, B.; Yang, F.; Zhang, T.; Wang, Y.; Wu, Z. Palynological assemblages of Beipiao Formation in Jinyang Basin of West Liaoning, and their age and Paleoclimatic significances. *Earth Sci.* **2019**, *44*, 3393–3408. (In Chinese with English Abstract)

50. Zhang, L.S.; Xie, M.Z.; Zhang, S.S.; Zhang, X.S.; Shang, H.T.; Li, X.H.; Wu, R.F. Rediscussion on geologic age and regional correlation about Beipiao Formation in Western Liaoning. *Geol. Rev.* **2016**, *62*, 1392–1402. (In Chinese with English Abstract)
51. Gao, H.-L.; Zhao, Y.; Zhang, S.-H.; Liu, J.; Ye, H.; Wang, G.-C. Ages of Jurassic volcano-sedimentary strata in the Yanshan Fold-and-Thrust Belt and their implications for the coal-bearing strata of northern China. *Int. Geol. Rev.* **2018**, *61*, 956–971. [[CrossRef](#)]
52. Peters, K.E.; Cassa, M.R. Applied Source Rock Geochemistry. In *The Petroleum System from Source to Trap*; Magoon, L.B., Dow, W.G., Eds.; The American Association of Petroleum Geologists: Tulsa, OK, USA, 1994; Volume 60, pp. 93–120.
53. Douville, E.; Bienvenu, P.; Charlou, J.L.; Donval, J.P.; Fouquet, Y.; Appriou, P.; Gamo, T. Yttrium and rare earth elements in fluids from various deep-sea hydrothermal systems. *Geochim. Cosmochim. Acta* **1999**, *63*, 627–643. [[CrossRef](#)]
54. Craddock, P.R.; Bach, W.; Seewald, J.S.; Rouxel, O.J.; Reeves, E.; Tivey, M.K. Rare earth element abundances in hydrothermal fluids from the Manus Basin, Papua New Guinea: Indicators of sub-seafloor hydrothermal processes in back-arc basins. *Geochim. Cosmochim. Acta* **2010**, *74*, 5494–5513. [[CrossRef](#)]
55. Chu, C.L.; Chen, Q.L.; Zhang, B.; Shi, Z.; Jiang, H.J.; Yang, X. Influence on formation of Yuertusi source rock by hydrothermal activities at Dongergou section, Tarim Basin. *Acta Sedimentol. Sin.* **2016**, *34*, 803–810. (In Chinese with English Abstract)
56. Peters, K.E.; Walters, C.C.; Moldowan, J.M. *The Biomarker Guide: Biomarkers and Isotopes in Petroleum Exploration and Earth History*, 2nd ed.; Cambridge University Press: Cambridge, UK, 2005; Volume 2.
57. George, S. Effect of igneous intrusion on the organic geochemistry of a siltstone and an oil shale horizon in the Midland Valley of Scotland. *Org. Geochem.* **1992**, *18*, 705–723. [[CrossRef](#)]
58. Cronan, D.; Varnavas, S.; Perissoratis, C. Hydrothermal sedimentation in the caldera of Santorini, Hellenic Volcanic Arc. *Terra Nova* **1995**, *7*, 289–293. [[CrossRef](#)]
59. Hecht, L.; Freiburger, R.; Gilg, H.A.; Grundmann, G.; Kostitsyn, Y.A. Rare earth element and isotope (C, O, Sr) characteristics of hydrothermal carbonates: Genetic implications for dolomite-hosted talc mineralization at Göpfersgrün (Fichtelgebirge, Germany). *Chem. Geol.* **1999**, *155*, 115–130. [[CrossRef](#)]
60. Hu, W.X.; Chen, Q.; Wang, X.L.; Cao, J. REE models for the discrimination of fluids in the formation and evolution of dolomite reservoirs. *Oil Gas Geol.* **2010**, *31*, 810–818. (In Chinese with English Abstract)
61. Hu, W.X. Origin and indicators of deep-seated fluids in sedimentary basins. *Bull. Miner. Petrol. Geochem.* **2016**, *35*, 817–826. (In Chinese with English Abstract)
62. Bau, M.; Schmidt, K.; Koschinsky, A.; Hein, J.; Kuhn, T.; Usui, A. Discriminating between different genetic types of marine ferro-manganese crusts and nodules based on rare earth elements and yttrium. *Chem. Geol.* **2014**, *381*, 1–9. [[CrossRef](#)]
63. Espitalié, J.; Laporte, J.L.; Madec, M.; Marquis, F.; Leplat, P.; Pauletand, J.; Boutefeu, A. Methode rapide de caracterisation des roches meres, de leur potentiel petrolier et de leur degre d'évolution. *Rev. Inst. Fr. Petrol.* **1977**, *32*, 23–42. [[CrossRef](#)]
64. Peters, K.E. Guidelines for Evaluating Petroleum Source Rock Using Programmed Pyrolysis. *AAPG Bull.* **1986**, *70*, 318–329. [[CrossRef](#)]
65. Langford, F.F.; Blanc-Valleron, M. Interpreting Rock-Eval pyrolysis data using graphs of pyrolyzable hydrocarbons vs. total organic carbon. *AAPG (Am. Assoc. Pet. Geol.) Bull.* **1990**, *74*, 799–804.
66. Svensen, H.; Planke, S.; Chevallier, L.; Malthe-Sørenssen, A.; Corfu, F.; Jamtveit, B. Hydrothermal venting of greenhouse gases triggering Early Jurassic global warming. *Earth Planet. Sci. Lett.* **2007**, *256*, 554–566. [[CrossRef](#)]
67. Aarnes, I.; Svensen, H.; Polteau, S.; Planke, S. Contact metamorphic devolatilization of shales in the Karoo Basin, South Africa, and the effects of multiple sill intrusions. *Chem. Geol.* **2011**, *281*, 181–194. [[CrossRef](#)]
68. Bishop, A.N.; Abbott, G.D. Vitrinite reflectance and molecular geochemistry of Jurassic sediments: The influence of heating by Tertiary dykes (northwest Scotland). *Org. Geochem.* **1995**, *22*, 165–177. [[CrossRef](#)]
69. Iyer, K.; Schmid, D.W. Comment on “Thickness matters: Influence of dolerite sills on the thermal maturity of surrounding rocks in a coal bed methane play in Botswana” by Bulguroglu and Milkov (2020). *Mar. Pet. Geol.* **2020**, *115*, 104247. [[CrossRef](#)]
70. Wang, D. Comparable study on the effect of errors and uncertainties of heat transfer models on quantitative evaluation of thermal alteration in contact metamorphic aureoles: Thermophysical parameters, intrusion mechanism, pore-water volatilization and mathematical equations. *Int. J. Coal Geol.* **2012**, *95*, 12–19. [[CrossRef](#)]
71. Aquino Neto, F.R.; Trendel, J.M.; Restle, A.; Connan, J.; Albrecht, P. Occurrence and Formation of Tricyclic and Tetracyclic Terpanes in Sediments and Petroleum. In *Advances in Organic Geochemistry, Bjorøy, M., Ed.*; Wiley: Hoboken, NJ, USA, 1981; pp. 659–667.
72. Neto, F.A.; Trigüis, J.; Azevedo, D.; Rodrigues, R.; Simoneit, B. Organic geochemistry of geographically unrelated tasmanites. *Org. Geochem.* **1992**, *18*, 791–803. [[CrossRef](#)]
73. Zumberge, J.E. Prediction of source rock characteristics based on terpane biomarkers in crude oils: A multivariate statistical approach. *Geochim. Cosmochim. Acta* **1987**, *51*, 1625–1637. [[CrossRef](#)]
74. Hanson, A.D.; Zhang, S.C.; Moldowan, J.M.; Liang, D.G.; Zhang, B.M. Molecular organic geochemistry of the Tarim basin, NW China. *AAPG (Am. Assoc. Pet. Geol.) Bull.* **2000**, *84*, 1109–1128.
75. Volk, H.; George, S.C.; Dutkiewicz, A.; Ridley, J. Characterisation of fluid inclusion oil in a Mid-Proterozoic sandstone and dolerite (Roper Superbasin, Australia). *Chem. Geol.* **2005**, *223*, 109–135. [[CrossRef](#)]
76. Noble, R.A.; Alexander, R.; Kagi, R.I.; Knox, J. Tetracyclic diterpenoid hydrocarbons in some Australian coals, sediments and crude oils. *Geochim. Cosmochim. Acta* **1985**, *49*, 2141–2147. [[CrossRef](#)]

77. Azevedo, D.; Neto, F.R.A.; Simoneit, B.; Pinto, A. Novel series of tricyclic aromatic terpanes characterized in Tasmanian tasmanite. *Org. Geochem.* **1992**, *18*, 9–16. [[CrossRef](#)]
78. Volkman, J.K. A review of sterol markers for marine and terrigenous organic matter. *Org. Geochem.* **1986**, *9*, 83–99. [[CrossRef](#)]
79. Grantham, P.; Wakefield, L. Variations in the sterane carbon number distributions of marine source rock derived crude oils through geological time. *Org. Geochem.* **1988**, *12*, 61–73. [[CrossRef](#)]
80. Volkman, J.K.; Barrett, S.M.; Blackburn, S.I.; Mansour, M.P.; Sikes, E.L.; Gelin, F. Microalgal biomarkers: A review of recent research developments. *Org. Geochem.* **1998**, *29*, 1163–1179. [[CrossRef](#)]
81. Knoll, A.H.; Summons, R.E.; Waldbauer, J.R.; Zumberge, J.E. The Geological Succession of Primary Producers in the Oceans. In *The Evolution of Primary Producers in the Sea*; Falkowski, P., Knoll, A.H., Eds.; Academic Press: Boston, MA, USA, 2007; pp. 133–163. [[CrossRef](#)]
82. Huang, W.-Y.; Meinschein, W. Sterols as ecological indicators. *Geochim. Cosmochim. Acta* **1979**, *43*, 739–745. [[CrossRef](#)]
83. Bohacs, K.M.; Carroll, A.R.; Neal, J.E.; Mankiewicz, P.J. Lake-Basin Type, Source Potential, and Hydrocarbon Character: An Integrated Sequence-Stratigraphicgeochemical Framework. In *Lake Basins through Space and Time*; Gierlowski-Kordesch, E.H., Kelts, K.R., Eds.; American Association of Petroleum Geologists Studies in Geology: Tulsa, OK, USA, 2000; Volume 46, pp. 3–34.
84. Gonçalves, F.T.T. Organic and isotope geochemistry of the Early Cretaceous rift sequence in the Camamu Basin, Brazil: Paleolimnological inferences and source rock models. *Org. Geochem.* **2002**, *33*, 67–80. [[CrossRef](#)]
85. Goodwin, N.; Mann, A.; Patience, R. Structure and significance of C30 4-methyl steranes in lacustrine shales and oils. *Org. Geochem.* **1988**, *12*, 495–506. [[CrossRef](#)]
86. Volkman, J.K.; Farmer, C.L.; Barrett, S.M.; Sikes, E.L. Unusual dihydroxysterols as chemotaxonomic markers for microalgae from the order pavlovales (haptophyceae). *J. Phycol.* **1997**, *33*, 1016–1023. [[CrossRef](#)]
87. Hou, D.; Wang, T.; Kong, Q.; Feng, Z.; Moldowan, J.M. Distribution and characterization of C31 sterane from cretaceous sediments and oils, Songliao Basin, China. *Chin. Sci. Bull.* **1999**, *44*, 560–563. [[CrossRef](#)]
88. Thomas, J.; Marshall, J.; Mann, A.; Summons, R.; Maxwell, J. Dinosteranes (4,23,24-trimethylsteranes) and other biological markers in dinoglagellate-rich marine sediments of Rhaetian age. *Org. Geochem.* **1993**, *20*, 91–104. [[CrossRef](#)]
89. Xiao, H.; Li, M.J.; Yang, Z.; Zhu, Z.L. Distribution patterns and geochemical implications of C19–C23 tricyclic terpanes in source rocks and crude oils occurring in various depositional environments. *Acta Geochim.* **2019**, *48*, 161–170. (In Chinese with English Abstract)
90. Didyk, B.M.; Simoneit, B.R.T.; Brassell, S.C.; Eglinton, G. Organic geochemical indicators of palaeoenvironmental conditions of sedimentation. *Nature* **1978**, *272*, 216–222. [[CrossRef](#)]
91. Mello, M.R.; Telnaes, N.; Caglianone, P.C.; Chicarelli, M.I.; Brassell, S.C.; Maxwell, J.R. Organic geochemical characterization of depositional palaeoenvironments of source rocks and oils in Brazilian marginal basins. *Org. Geochem.* **1988**, *13*, 31–45. [[CrossRef](#)]
92. Damsté, J.S.S.; Kenig, F.; Koopmans, M.P.; Köster, J.; Schouten, S.; Hayes, J.; de Leeuw, J.W. Evidence for gammacerane as an indicator of water column stratification. *Geochim. Cosmochim. Acta* **1995**, *59*, 1895–1900. [[CrossRef](#)]